Evaluating cooling and energy-saving potential of Vertical Greenery Systems based on 3D City Models: A case study of three cities

Chengjie Li[1], Zhe Chen[1], Fuxun Liang[1,2], Zhen Dong[1], Bisheng Yang[1]

[1] State Key Laboratory of Information Engineering in Surveying, Mapping and Remote Sensing (LIESMARS),
Wuhan University, Wuhan, China
[2] School of Urban Design, Wuhan University, Wuhan, China

Keywords: 3D city models, Urban morphology, Urban microclimate, Vertical Greenery Systems.

Abstract

Global cities face escalating urban heat stress and energy demands due to rapid vertical growth and densification. Vertical Greenery Systems (VGS), which mitigate urban heat by providing shading and evapotranspiration, offering a promising nature-based solution to enhance environmental sustainability. 3D city models serve as a suitable tool for simulating VGS due to their precise representation of urban environments. However, research leveraging 3D city models in VGS simulations is still limited. To address this challenge, this study evaluates the cooling and energy-saving potential of VGS using 3D city models in Wuhan, Hong Kong, and Singapore. A novel workflow encompassing microclimate simulation, solar irradiation calculation, and view factors computation is developed to assess VGS's performance over 24 hours on a typical summer day, June 21st. Cooling and energy-saving performance are subsequently estimated. Our study highlights that VGS's performance strongly correlates with climatic background and urban morphology, offering valuable insights for promoting and optimizing VGS deployment. By pioneering the integration of 3D city models with VGS, this study establishes a foundation for future multi-seasonal and city-scale VGS simulations.

1. Introduction

Global cities have increasingly replaced horizontal expansion with vertical growth (Frolking et al., 2024). The reshaped 3D urban structures significantly influence urban microclimate, such as altering ventilation in street canyons. Coupled with rapid urbanization that leads to urban densification (Erlwein et al., 2021), these changes exacerbate urban warming (Li et al., 2023) and amplify urban energy burdens.

As green interventions are proved to be effective nature-based solutions against urban heat stress (Ouyang et al., 2023; Oorschot et al., 2024), urban greening has long been promoted by governments. Nevertheless, available land for green spaces is limited in dense urban areas (Zhang et al., 2022). Vertical Greenery Systems (VGS), which integrate vegetation into building facades, effectively utilize underused facade spaces (Alexandri and Jones, 2008; Peng et al., 2020; Rupasinghe and Halwatura, 2020). VGS primarily benefit buildings and their surroundings through shading, evapotranspiration, and insulation (Koch et al., 2020). For instance, VGS reduce cooling demand by intercepting solar irradiation on building walls (Wong et al., 2021). In addition, plants cool surrounding air by converting sensible heat into latent heat through transpiration (Hoelscher et al., 2016). Given their thermal and energy benefits, VGS provide a practical solution to mitigate urban warming and reduce building energy consumption.

Previous studies have employed field measurements and simulations to assess the thermal impact and energy-saving potential of VGS. For example, Wong et al. (2010) carried on an experiment in Singapore, indicating that VGS reduce ambient temperature by 3.33°C at a distance of 0.15 m. However, since the lack of large-scale VGS deployment in the real world (Peng et al., 2020), field measurements are currently incapable of capturing cumulative cooling effects at greater distances. Regarding simulations, researchers have developed numerical models for

VGS. Stec et al. (2005) modeled the physical processes of VGS base on thermal network model, whereas Susorova et al. (2013) proposed a mathematical model simulating one-dimensional heat flux through vegetated facades. Though numerical models can account for various factors affecting VGS's performance, particularly across different climatic zones, their reliance on coarse weather data limits their ability to characterize detailed local microclimate. Several attempts have integrated numerical models with building energy simulation (BES) tools to further investigate the energy performance of VGS. Larsen et al. (2015) proposed a simplified method that treats VGS as a shading material in EnergyPlus, embedding a thermal model of VGS into the software. Djedjig et al. (2015) developed a heat and moisture transfer model of VGS, before integrating into the transient building simulation program (TRNSYS). But these studies did not carry on a simulation beyond the building scale. Aiming at capturing the intricate interactions between VGS and microclimate, simulations based on computational fluid dynamics (CFD) have been performed. ENVI-met, a widely used CFD software for urban climate, have been employed by previous studies to quantify cooling and energy performance of VGS (Morakinyo et al., 2019; Peng et al., 2020; Daemei et al., 2021). Nonetheless, the computational cost is the main barrier to extending CFD simulations from block-scale to larger scales. Thus, hitherto the cooling and energy-saving potential of VGS beyond block-scale remains unrealized.

3D city models provide digital representations of urban environments (Biljecki et al., 2015), precisely characterize 3D urban morphology, supporting accurate analysis of microclimatic conditions and shadowing effects (Willenborg et al., 2017), which is crucial for VGS simulation. Besides, based on the geometry of 3D city models, the energy flows can be analyzed, particularly heat transfer through building walls. Meanwhile, VGS simulation offers a new approach for expanding application domains of 3D city models. Other than visualization, 3D city models have been applicated to solar photovoltaic potential es-

timation (Zhu et al., 2020; Chen et al., 2024), noise propagation analysis (Stoter et al., 2008; Guo et al., 2023), explosion simulation (Willenborg, 2015; Shi et al., 2025), and 3D cadastre (Stoter et al., 2013; Paasch and Paulsson, 2021). However, studies that integrate 3D city models and assess VGS's potential remain scarce and typically confined to small scales via CFD-based approaches (Teichmann et al., 2022).

Furthermore, due to the varying climatic conditions and dominant urban morphologies, the cooling and energy-saving potential that VGS bring are heterogeneous across cities. Exploring the correlations between climate background, urban morphology and VGS's cooling and energy-saving potential can facilitate optimal deployment.

In this study, we bridge the gap between 3D city models and VGS. We first develop a VGS simulation workflow (as shown in Figure 1), allowing VGS simulation in large scale simulations over 24 hours on a typical summer day, which will be elaborated in the next section. Next, simulations of Wuhan, Hong Kong, and Singapore are conducted.

2. Methods

We employ a numerical model (Susorova et al., 2013) based on the energy balance of VGS. 3D city models are superimposed upon the terrain, and building facades from the models are extracted and subsequently subdivided into 1-meter grid cells using Ladybug Tools (Figure 2). To obtain the corresponding fine-grained parameters as inputs for the model, we implement three major components: microclimate simulation, solar irradiation calculation and view factors computation.

2.1 Study area and data

The workflow is applied to Wuhan (Humid subtropical climate, Cfa), Hong Kong (Monsoon-influenced humid subtropical climate, Cwa), and Singapore (Tropical rainforest climate, Af), representing distinct climates in Köppen climate classification with varying dominant urban morphologies. Building footprints from OpenStreetMap which will be extruded to 3D city models, digital elevation models (DEM) from EarthData, and meteorological data from ERA5 are collected.

2.2 Numerical modelling

The numerical model comprises long-wave radiation, short-wave radiation, sensible heat flux, and latent heat flux for building walls with and without VGS. The energy balance equations for bare wall (Eq. 1), vegetated wall (Eq. 2), and foliage (Eq. 3) are given as:

$$LR_{bw} + SR_{bw} = Q_{bw} + C_{bw} + S_{bw} \tag{1}$$

$$LR_{vw} + SR_{vw} - XR = Q_{vw} + C_{vw} + S_{vw} \tag{2}$$

$$LR_{leaf} + SR_{leaf} + XR = L_{leaf} + C_{leaf} \tag{3}$$

where LR is the long-wave radiation, which contributes to the total incoming radiation together with short-wave radiation SR

from the external environment. XR represents the radiative exchange between the plant and building wall. Q and C denote conductive and convective heat fluxes, respectively. L is the latent heat flux of the plant, and S is the energy stored in the building wall. The long-wave radiation of bare wall (Eq. 2.2), vegetated wall (Eq. 2.2), and foliage (Eq. 2.2) are calculated as:

$$LR_{bw} = \epsilon_{wall}\epsilon_{sky}\sigma F_{sky}(T_{sky}^4 - T_{sbw}^4) +$$
$$\epsilon_{wall}\epsilon_{gr}\sigma F_{gr}(T_{gr}^4 - T_{sbw}^4) \tag{4}$$

$$LR_{vw} = \epsilon_{wall}\epsilon_{sky}\sigma F_{sky}(T_{sky}^4 - T_{svw}^4) +$$
$$\epsilon_{wall}\epsilon_{gr}\sigma F_{gr}(T_{gr}^4 - T_{svw}^4) +$$
$$\tau\epsilon_{wall}\epsilon_{leaf}\sigma F_{bld}(T_{leaf}^4 - T_{svw}^4) \tag{5}$$

$$LR_{leaf} = (1 - \tau)\epsilon_{leaf}\epsilon_{sky}\sigma F_{sky}(T_{sky}^4 - T_{leaf}^4) +$$
$$(1 - \tau)\epsilon_{leaf}\epsilon_{gr}\sigma F_{gr}(T_{gr}^4 - T_{leaf}^4) +$$
$$\tau\epsilon_{wall}\epsilon_{leaf}\sigma F_{bld}(T_{svw}^4 - T_{leaf}^4) \tag{6}$$

where ϵ is the emissivity, σ is the Stefan-Boltzmann constant (5.67×10^{-8} W/m^2 K^4), T denotes the temperatures of sky, leaf, and exterior surface of the wall, and τ is the transmissivity of radiation through the plant. The short-wave radiation of bare wall (Eq. 7), vegetated wall (Eq. 8), and foliage (Eq. 9) are given by the following equations:

$$SR_{bw} = \alpha_{wall}I_s \tag{7}$$

$$SR_{vw} = \alpha_{wall}(1 - \tau)I_s \tag{8}$$

$$SR_{leaf} = \alpha_{leaf}(1 - \tau)I_{solar} \tag{9}$$

where I_s is the solar irradiation received by the facade, α is the solar absorptivity. Conductive and convective heat fluxes are two forms of sensible heat flux. The conductive heat flux for bare wall (Eq. 10) and vegetated wall (Eq. 11) are expressed as:

$$Q_{bw} = (T_{sbw} - T_{in})/R_{bw} \tag{10}$$

$$Q_{vw} = (T_{svw} - T_{in})/R_{vw} \tag{11}$$

where T_{in} is the interior surface temperature of the wall, R denotes the thermal resistance of the wall. The convective heat flux for bare wall (Eq. 12), vegetated wall (Eq. 13), and foliage (Eq. 14) are calculated by:

$$C_{bw} = \rho_a c_p b v_a (T_a - T_{sbw}) \tag{12}$$

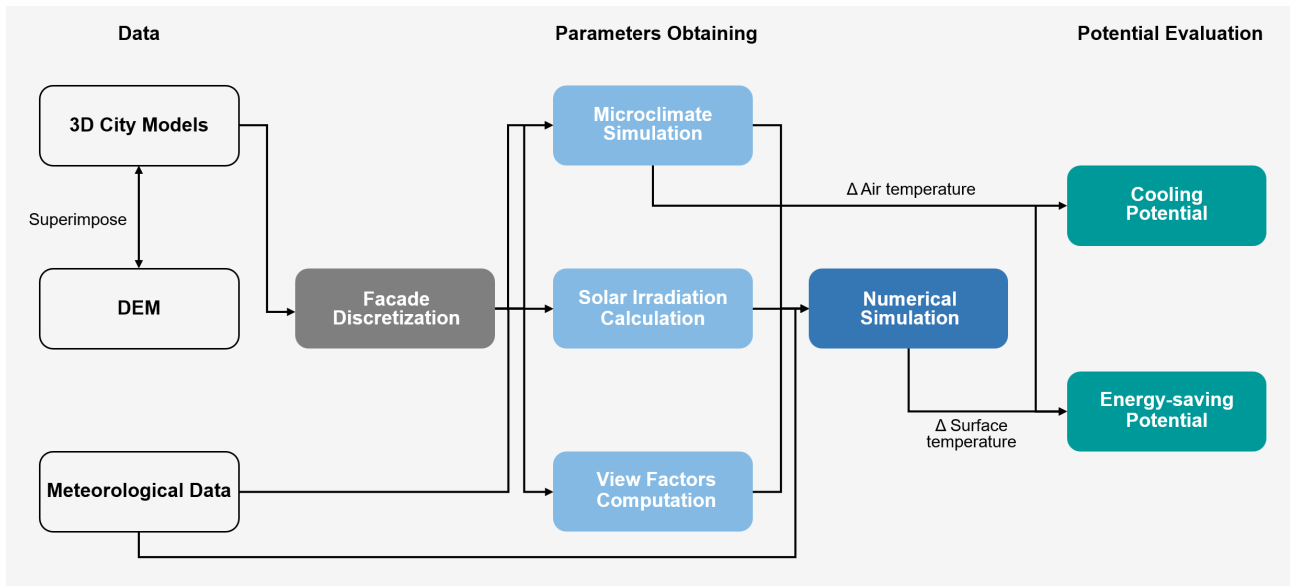$$C_{vw} = \rho_a c_p b v_a (T_a - T_{svw}) \tag{13}$$

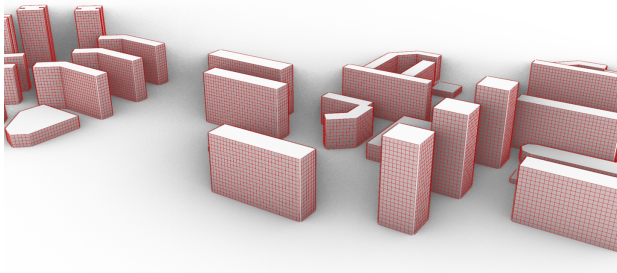Figure 1. The comprehensive workflow for VGS simulation.

Figure 2. Subdividing building facades into 1-meter grid cells using Ladybug Tools.

$$C_{leaf} = 1.1 LAI \rho_a c_p b v_a (T_a - T_{leaf}) \qquad (14)$$

where ρ_a is the air density, v_a is the wind speed, T_a is the temperature within the foliage, c_p is the specific heat at constant pressure, b is bulk heat transfer coefficient, and LAI is the leaf area index. The evapotranspiration of the plant is calculated based on Penman-Monteith equation (Eq. 15), followed by the latent heat flux presented as Eq. 16.

$$E = \frac{\Delta (R_n - G) + \rho c_p (e_s - e_a)/r_a}{\lambda(\Delta + \gamma(1 + r_s/r_a))} \qquad (15)$$

$$L_{leaf} = \lambda E \qquad (16)$$

where R_n is the net radiation balance, G is the vapor pressure, Δ is the slope of the saturation vapor pressure-temperature relationship, γ is a psychrometric constant, and λ is a repartition coefficient.

The numerical model is solved by employing Newton-Raphson method in conjunction with CuPy to derive the exterior surface temperature of each grid cell, allowing further evaluation of the reduced heat flux through the wall as a result of the shading

effect of VGS (Susorova et al., 2013). By combining differences between air temperature and indoor temperature to estimate heat removal rate, we assessed the total reduction in building energy consumption.
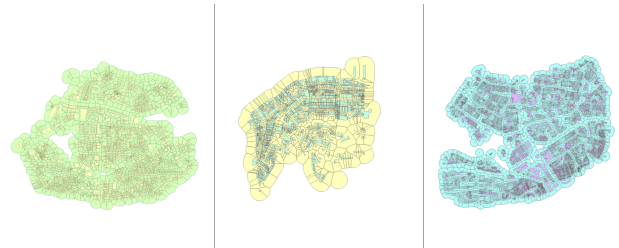

Figure 3. Voronoi tessellation for the three cities, Wuhan (left), Hong Kong (middle), and Singapore (right).

2.3 Microclimate simulation

First, to divide the whole region into spatially adjacent units for each building, we use the momepy Python library (Fleischmann et al., 2020) that applies Voronoi tessellation on polygons (Figure 3). Taking advantage of spatially adjacent Voronoi tessellations units, neighboring buildings with similar morphological characteristics are clustered into homogeneous units (in Figure 4) through Spatially Constrained Multivariate Clustering tool in ArcGIS Pro (Yang et al., 2024). Average morphological parameters for each homogeneous unit, including building height, orientation, roof width, and canyon width, are calculated. Subsequently, the averaged morphological parameters are fed into the Vertical City Weather Generator (VCWG), an urban canopy model (UCM) that provides high-fidelity vertical variation of microclimate variables (Moradi et al., 2022). The energy balance model of VGS is coupled with VCWG, reflecting their effects on microclimate.

The cooling potential is then quantified by comparing the air temperature at 1.5 meters of each homogeneous morphological unit before and after applying VGS.
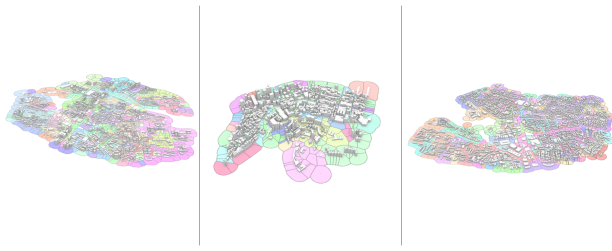
Figure 4. Clustering Voronoi tessellation units with similar morphological parameters, Wuhan (left), Hong Kong (middle), and Singapore (right).

2.4 Solar irradiation calculation

Giving the intention with both reducing computational cost and considering mutual shading, we partition the contiguous models into groups of fewer than 2100 elements. Models with minimum distance between the their centroids are agglomerated into a group. We create a minimum bounding box (MBB) for each group and compute the horizontal distance from its vertex to its center. The computed distance, extended by 100 meters, defines the radius of a circular region. Thereafter, buildings and terrain within this circular region are incorporated as shadowing objects to take into account their effects on peripheral models in the group. Moreover, we use the open source PVLIB-Python library to obtain the sunrise and sunset times. For each group, we employed Point-in-Time Grid-Based simulations in Ladybug Tools at the grid cell level, along with Accelerad which accelerates daylighting analysis on GPU. Thus, the solar irradiation on building facades is calculated for the diurnal period.

2.5 View factors computation

Third, view factors computation involves computing the sky view factor (SVF), building view factor (BVF), and ground view factor (GVF) of each grid cell. The SVF is derived via Sky View component in Ladybug Tools, applying Accelerad. Similarly, models for SVF computation are necessary to be grouped, which use the analogous partitioning method described in Section 2.4 for solar irradiation calculation.
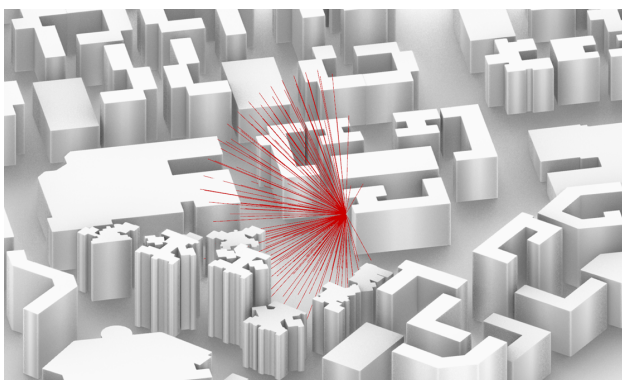

Figure 5. The hemisphere composed of rays.

Concerning BVF, a hemisphere composed of rays emitted from the center of each grid cell is constructed (Figure 5), prior to calculating the proportion of rays hitting buildings (Eq.17). The process is performed using the 'rtrace' command in the Radiance lighting simulation program. It should be noted that Ac-

celerad enables the speedup of ray-tracing with GPU.

$$F_{bld} = \frac{N_{hit}}{N_{total}} \qquad (17)$$

where N_{total} is the total number of rays, N_{hit} is the ray that hits the buildings.

After calculating SVF and BVF, GVF is determined by subtracting both from 1:

$$F_{gr} = 1 - F_{sky} - F_{bld} \qquad (18)$$

3. Results

3.1 Cooling Potential of VGS

The collected results from VCWG simulation indicating the cooling impacts of VGS focus on two perspectives: (1) the hourly average temperature reduction at a height of 1.5 meters across all homogeneous morphological units in the three cities, derived from hourly data, and (2) the spatial variation of cooling effects within each homogeneous morphological units at 1.5 meters at 14:00 across all three cities, providing insights to spatial and temporal distributions of VGS's cooling performance. The 24-hour temperature reduction profiles across Wuhan, Hong Kong, and Singapore, as depicted in Figure 6, exhibit consistent trends with notable cooling during the day and warming at night. The cooling effect begins to increase around 5:00 for Wuhan and Hong Kong, and 6:00 for Singapore, aligning with approximate sunrise time. For Wuhan and Hong Kong, temperature reductions rise steadily, peaking at 11:00 (0.4°C) and 10:00 (1.8°C), respectively, followed by a brief decline before reaching maximum reductions of 0.75°C at 14:00 and 2.5°C at 16:00. In Singapore, cooling effect increases continuously from 6:00 to 15:00, peaking at approximately 1.5°C. Subsequently, temperature reductions plummet before dusk, reaching -0.8°C, -0.75°C, and 0°C for Wuhan, Hong Kong, and Singapore, respectively, followed by a slight uptick and stabilize at midnight.

The spatial distribution of cooling effects at 14:00, illustrated in Figure 7, reveals distinct patterns across the three cities. In Wuhan, the implementation of VGS results in warming impacts mainly in areas with low-rise south-oriented buildings in the western part, whereas temperature reductions exceeding 4°C are observed in regions characterized by high-rise buildings. Moderate cooling (up to 1-2°C) is evident in low-rise, high-density homogeneous morphological units. In Hong Kong, most areas show positive cooling effects, with scattered areas warming up to -0.96°C in homogeneous morphological units characterized by low-rise zones adjacent to high-rise buildings in the southwestern part and low-rise, low-density areas in the southern part. Other regions exhibit temperature reductions ranging from 1.10°C in open spaces to 4.35°C in regions dominated by high-rise buildings with compact layouts. Singapore demonstrates a uniform cooling effect across all homogeneous morphological units, with temperature reductions ranging from 0.25°C in spacious areas to 4.38°C in the high-density zones. Given the study area's predominance of low-rise buildings, the highest cooling benefits are associated with compact layouts, while the lowest effects occur in less dense areas with larger building footprints. Such spatial patterns underscore the interplay between urban morphology and VGS cooling efficiency.
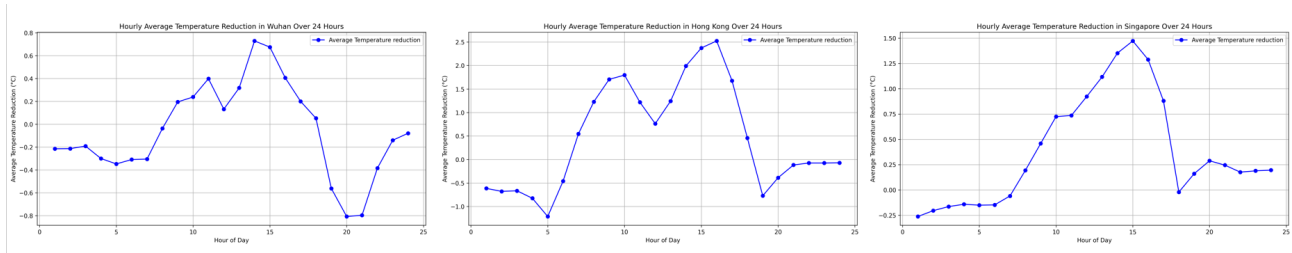
Figure 6. The hourly average temperature reduction across three cities, Wuhan (left), Hong Kong (middle), and Singapore (right).
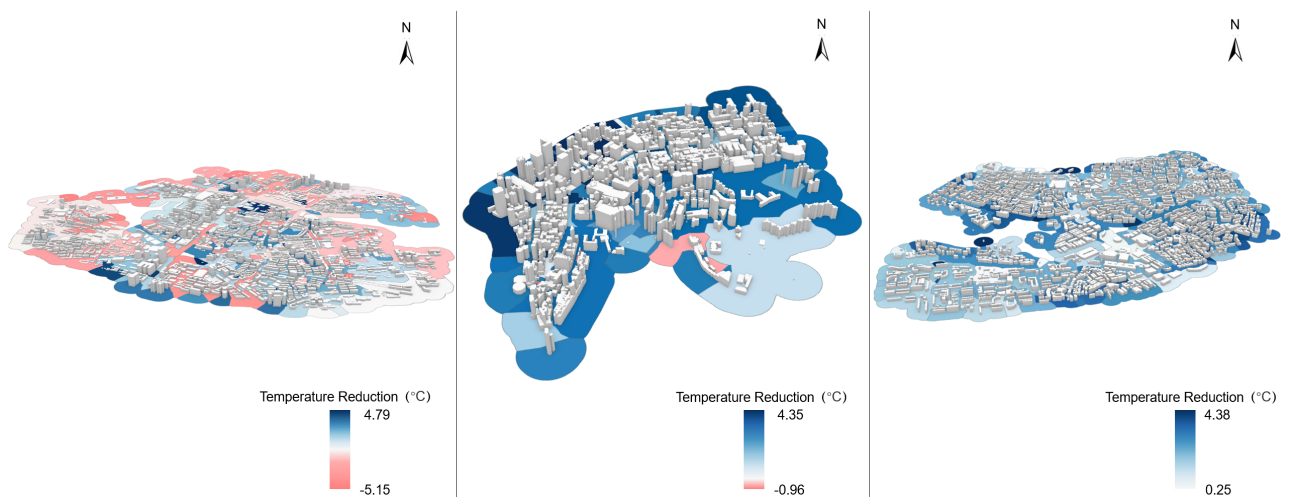

Figure 7. The spatial distribution of cooling effect in three cities, Wuhan (left), Hong Kong (middle), and Singapore (right).

3.2 Energy-Saving Potential of VGS

The grid-wise exterior wall surface temperature reductions at 14:00 for the three cities are presented in Figure 8. In Wuhan, temperature reductions range from 1.30°C to a maximum of 21.47°C, with the most significant reductions (>15°C) observed on the southwest-facing facades of high-rise buildings in the southern part of the study area. Moreover, remarkable reductions also extend to the lower floors of mid-rise buildings and low-rise structures, while reductions below 5°C are predominantly found on the upper floors of high-rise buildings. Hong Kong saw a range of 2.77°C to 26.09°C, with substantial cooling sporadically distributed on southwest-oriented facades in the southwestern region. A large proportion of buildings in the central area exhibit medium reductions (5°C to 20°C) on their lower floors, whereas upper floors of high-rise buildings show minimal reductions. Notably, reductions below 5°C are consistent across the entire facades of buildings along the northwestern edge. Singapore, reductions vary between 0.73°C and 27.15°C, with isolated instances of significant reductions (>20°C) in the southwestern part. Most grid cells display moderate reductions, while slight reductions (<5°C) are concentrated on the top floors of mid-rise buildings.

The energy-saving potential of VGS was estimated based on reductions in air temperature and facade exterior surface temperatures. For approximately 2,000 buildings on June 21st, VGS implementation is projected to reduce building energy consumption by -2.92 GWh in Wuhan, 72.07 GWh in Hong Kong, and 81.75 GWh in Singapore. The negative value in Wuhan suggests a potential increase in energy use, possibly due to the rainy weather.

4. Discussion

Our work presents an innovative workflow to evaluate the potential of applying VGS on building facades through 3D city models across diverse cities, laying a foundation for design guidelines. The cooling performance of VGS across Wuhan, Hong Kong, and Singapore demonstrates significant variations driven by climatic and morphological factors. The hourly temperature reductions decline from Hong Kong to Singapore to Wuhan, corresponding to the diminishing solar radiation intensity across three cities. This correlation suggests that the level of incoming solar irradiation enhances evapotranspiration, thereby significantly influencing the effectiveness of the cooling impact. Nighttime warming, most pronounced in Hong Kong followed by Wuhan, may result from suppressed plant transpiration and reduced outgoing long-wave radiation (Peng et al., 2020), exacerbated by heat retention in high-rise, high-density areas.

At 14:00, Wuhan's broadly distributed negative cooling impacts are presumably stems from rainfall and high humidity in Wuhan on June 21st, 2024, which suppresses plant evapotranspiration. In addition, the decreased ventilation might contribute to the observed warming effect. Conversely, regions with high-rise and southwest-facing low-rises buildings achieve temperature reductions exceeding 2°C, likely facilitated by the prevailing southwest wind direction, which amplifies ventilation
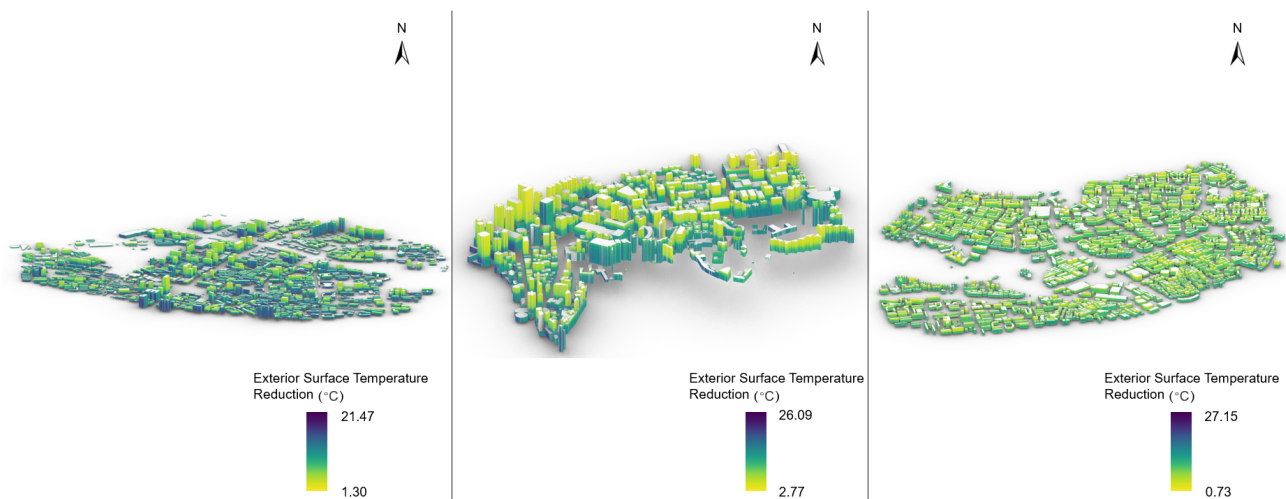
Figure 8. Building surface exterior temperature reduction in three cities(a subset of the whole area), Wuhan (left), Hong Kong (middle), and Singapore (right).

and thus boosts the cooling impact of VGS. Hong Kong's performance indicates that low-rise zones adjacent to high-rises experience heat retention due to reduced ventilation, while compact high-rise areas benefit most resulting from the large greening area, with up to 4.35°C. Singapore's uniform cooling impact is likely attributed to its predominantly low-rise building structure, which decreases mutual shading and enhances ventilation efficiency.

The exterior wall surface temperature reductions induced by VGS vary significantly across Wuhan, Hong Kong, and Singapore, showcasing the influence of local climate and urban morphology on the energy-saving potential of VGS. In Wuhan, temperature reductions on building exterior surfaces range from 1.30°C to 21.47°C, with relatively modest decreases attributed to rainfall diminishing the shading efficacy of VGS. To be specific, substantial reductions are observed on southwest-facing facades of high-rise buildings at the southern edge, which can be attributed to the more sun exposure blocked by VGS. Remarkable drops are also evident on low-rise buildings and the lower floors of mid-rise buildings, potentially resulting from reduced convective heat exchange with the atmosphere under lower wind speeds, fostering a cool, stagnant air layer between the VGS and building walls. In contrast, higher wind speeds at elevated floors of high-rise buildings enhance convective heat transfer, which may offset the shading benefits provided by VGS. In Hong Kong, temperature reductions range from 2.77°C to 26.09°C, with pronounced decreases on southwest-oriented facades in the southwestern region, driven by effective shading under intense solar radiation. Meanwhile, moderate reductions across most grid cells are attributed to mutual shading effects in high-density, high-rise urban blocks. In Singapore, temperature decreases vary from 0.73°C to 27.15°C, with most areas exhibiting moderate reductions between 5°C and 20°C. Such phenomenon is stemmed from reduced mutual shading among the predominant low-rise buildings, allowing VGS to exert more shading effects.

The findings suggest that cooling and energy-saving benefits strongly correlate with climatic background and urban morphology, which indicates the importance of tailored schemes for different cities. For example, low-rise low-density residential area in cities with hot climate and high solar irradiation

might substantively benefited from deploying VGS, due to the low mutual shading which leads to substantial energy-saving. It should be noted that since climatic background matters, the cross-seasonal influences of VGS deserve further exploration. In future research, we will incorporate multi-seasonal VGS simulation. Additionally, since the number of 3D city models our study is around 2000, a city scale VGS simulation should be further achieved for better exploring VGS's cooling and energy-saving patterns in different cities.

5. Conclusion

VGS offer a sustainable solution to mitigate urban heat stress and the inflating energy demands in rapidly urbanizing cities. This study proposed a novel workflow for assessing the cooling and energy-saving potential of VGS in Wuhan, Hong Kong, and Singapore, demonstrating both the capability and suitability of 3D city models for VGS simulation. The results indicate that VGS can mitigate urban warming and reduce energy consumption, with performance varying across different climatic conditions, urban morphologies and time of day. These findings highlight a promising strategy to utilize building facades and offer insights for urban planners to optimize the real-world deployment of VGS. Future research should extend the temporal dimension through multi-seasonal VGS simulation and expand the spatial scope to city-wide assessment.

References

Alexandri, E., and Jones, P., 2008. Temperature decreases in an urban canyon due to green walls and green roofs in diverse climates. *Building and Environment*, 43(4), 480-493.

Biljecki, F., Stoter, J., Ledoux, H., Zlatanova, S., and Çöltekin, A., 2015. Applications of 3D city models: State of the art review. *ISPRS International Journal of Geo-Information*, 4(4), 2842-2889.

Chen, Z., Yang, B., Zhu, R., and Dong, Z., 2024. City-scale solar PV potential estimation on 3D buildings using multi-source RS data: A case study in Wuhan, China. *Applied Energy*, 359, 122720.

Daemei, A. B., Shafiee, E., Chitgar, A. A., and Asadi, S., 2021. Investigating the thermal performance of green wall: Experimental analysis, deep learning model, and simulation studies in a humid climate. *Building and Environment*, 205, 108201.

Djedjig, R., Bozonnet, E., and Belarbi, R., 2015. Analysis of thermal effects of vegetated envelopes: Integration of a validated model in a building energy simulation program. *Energy and Buildings*, 86, 93-103.

Erlwein, S., Zölch, T., and Pauleit, S., 2021. Regulating the microclimate with urban green in densifying cities: Joint assessment on two scales. *Building and Environment*, 205, 108233.

Fleischmann, M., Feliciotti, A., Romice, O., and Porta, S., 2020. Morphological tessellation as a way of partitioning space: Improving consistency in urban morphology at the plot scale. *Computers, Environment and Urban Systems*, 80, 101441.

Frolking, S., Mahtta, R., Milliman, T., Esch, T., and Seto, K. C., 2024. Global urban structural growth shows a profound shift from spreading out to building up. *Nature Cities*, 1(9), 555-566.

Guo, M., Ni, M. Y., Shyu, R. J., Ji, J. S., and Huang, J., 2023. Automated simulation for household road traffic noise exposure: Application and field evaluation in a high-density city. *Computers, Environment and Urban Systems*, 104, 102000.

Hoelscher, M. T., Nehls, T., Jänicke, B., and Wessolek, G., 2016. Quantifying cooling effects of facade greening: Shading, transpiration and insulation. *Energy and Buildings*, 114, 283-290.

Koch, K., Ysebaert, T., Denys, S., and Samson, R., 2020. Urban heat stress mitigation potential of green walls: A review. *Urban Forestry & Urban Greening*, 55, 126843.

Larsen, S. F., Filippín, C., and Lesino, G., 2015. Modeling double skin green façades with traditional thermal simulation software. *Solar Energy*, 121, 56-67.

Li, X., Yang, B., Liang, F., Zhang, H., Xu, Y., and Dong, Z., 2023. Modeling urban canopy air temperature at city-block scale based on urban 3D morphology parameters–A study in Tianjin, North China. *Building and Environment*, 230, 110000.

Moradi, M., Krayenhoff, E. S., and Aliabadi, A. A., 2022. A comprehensive indoor–outdoor urban climate model with hydrology: The Vertical City Weather Generator (VCWG v2.0.0). *Building and Environment*, 207, 108406.

Morakinyo, T. E., Lai, A., Lau, K. K. L., and Ng, E., 2019. Thermal benefits of vertical greening in a high-density city: Case study of Hong Kong. *Urban Forestry & Urban Greening*, 37, 42-55.

Ouyang, W., Morakinyo, T. E., Lee, Y., Tan, Z., Ren, C., and Ng, E., 2023. How to quantify the cooling effects of green infrastructure strategies from a spatio-temporal perspective: Experience from a parametric study. *Landscape and Urban Planning*, 237, 104808.

Paasch, J. M., and Paulsson, J., 2021. 3D property research from a legal perspective revisited. *Land*, 10(5), 494.

Peng, L. L., Jiang, Z., Yang, X., He, Y., Xu, T., and Chen, S. S., 2020. Cooling effects of block-scale facade greening and their relationship with urban form. *Building and Environment*, 169, 106552.

Peng, L. L., Jiang, Z., Yang, X., Wang, Q, He, Y., and Chen, S. S., 2020. Energy savings of block-scale facade greening for different urban forms. *Applied Energy*, 279, 115844.

Rupasinghe, H. T., and Halwatura, R. U., 2020. Benefits of implementing vertical greening in tropical climates. *Urban Forestry & Urban Greening*, 53, 126708.

Shi, J., Li, J., Zhang, H., Xie, B., Xie, Z., Yu, Q., and Yan, J., 2025. Real-time gas explosion prediction at urban scale by GIS and graph neural network. *Applied Energy*, 377, 124614.

Stec, W. J., van Paassen, A. H. C., and Maziarz, A., 2005. Modelling the double skin façade with plants. *Energy and Buildings*, 37(5), 419-427.

Stoter, J., De Kluijver, H., and Kurakula, V., 2008. 3D noise mapping in urban areas. *International Journal of Geographical Information Science*, 22(8), 907-924.

Stoter, J., Ploeger, H., and van Oosterom, P., 2013. 3D cadastre in the Netherlands: Developments and international applicability. *Computers, Environment and Urban Systems*, 40, 56-67.

Susorova, I., Angulo, M., Bahrami, P., and Stephens, B., 2013. A model of vegetated exterior facades for evaluation of wall thermal performance. *Building and Environment*, 67, 1-13.

van Oorschot, J., Slootweg, M., Remme, R. P., Sprecher, B., and van der Voet, E., 2024. Optimizing green and gray infrastructure planning for sustainable urban development. *NPJ Urban Sustainability*, 4(1), 41.

Willenborg, B., 2015. Simulation of explosions in urban space and result analysis based on CityGML City models and a cloud based 3D Web client.

Willenborg, B., Sindram, M., and Kolbe, T. H., 2017. Applications of 3D city models for a better understanding of the built environment. *Trends in spatial analysis and modelling: decision-support and planning strategies*, 167-191.

Wong, N. H., Tan, A. Y. K., Chen, Y., Sekar, K., Tan, P. Y., Chan, D., ... and Wong, N. C., 2010. Thermal evaluation of vertical greenery systems for building walls. *Building and Environment*, 45(3), 663-672.

Wong, N. H., Tan, C. L., Kolokotsa, D. D., and Takebayashi, H., 2021. Greenery as a mitigation and adaptation strategy to urban heat. *Nature Reviews Earth & Environment*, 2(3), 166-181.

Yang, L., Chen, Y., Li, Y., Zhu, H., Yang, X., Li, S., and Tang, G., 2024. Is 3D building morphology really related to land surface temperature? Insights from a new homogeneous unit. *Building and Environment*, 266, 112101.

Zhang, J., Li, Z., Wei, Y., and Hu, D., 2022. The impact of the building morphology on microclimate and thermal comfort-a case study in Beijing. *Building and Environment*, 223, 109469.

Zhu, R., Wong, M. S., You, L., Santi, P., Nichol, J., Ho, H. C., ... and Ratti, C., 2020. The effect of urban morphology on the solar capacity of three-dimensional cities. *Renewable Energy*, 153, 1111-1126.